Supplementary Information

Hollow POM@MOF Hybrids-Derived Porous $Co_3O_4/CoMoO_4$ Nanocages for Enhanced Electrocatalytic Water Oxidation

Linjie Zhang, Taoqing Mi, Muhammad Asad Ziaee, Linfeng Liang, Ruihu Wang*

Supplementary Experimental Details

Tafel Slope Calculation of the Catalysts: The Tafel slope of the catalyst is calculated based on the Tafel equation:

$\eta = a + b \times \log j$

where η is overpotential in V, a is the Tafel constant in V, b is the Tafel slope in V dec^{-1} and j is the current density in A cm^{-2}. The Tafel plot was drawn by plotting overpotential as a function of the current density in logarithm, and the slope of the linear region is the Tafel slope.

Electrochemically Active Surface Area (ECSA) Calculation of the Catalyst: The ECSA of the catalyst is calculated from the double-layer capacitance according to the following equation:

$\mathrm{ECSA} = R_f \times S$

$R_f = C_{dl} / C_s$

where S is the geometric area of the smooth surface of the glassy carbon (GC) electrode (in this work, S = 0.196 cm^2) and R_f is the roughness factor calculated from the ratio of double-layer capacitance (C_{dl}) for the working electrode and the corresponding smooth GC electrode, C_{dl} is the slope of plots for the anodic or cathodic current density against scan rates in the non-Faradaic region, C_s is measured by a similar method only without modifying the catalyst. Therefore, the comparison of ECSA can be replaced by the comparison of C_{dl} value.

Turnover Frequency (TOF) Calculation of the Catalyst: The TOF value is calculated from the equation:

$\mathrm{TOF} = J \times A / (4 \times F \times n)$

where J is the current density at a specific overpotential in A cm^{-2}; A is the area of the GCE; F is the Faraday constant with a value of 96485 C mol^{-1}; and n is the number of moles of the active metal sites of the catalyst drop-cast on the electrode.

Faradaic Efficiency (ε) Calculation: The ε value is calculated from the equation:

$\varepsilon = I_{ring} / (I_{disk} \times N)$

where I_{disk} denotes the disk current, I_{ring} stands for the ring current, and N represents the current collection efficiency of the RRDE that is about 0.37 (Φ_{disk} and Φ_{ring} are 0.2475 and 0.1866 cm^2, respectively. And the interval between glass carbon disk and Pt ring electrodes is 318 μm).

Supplementary Figures

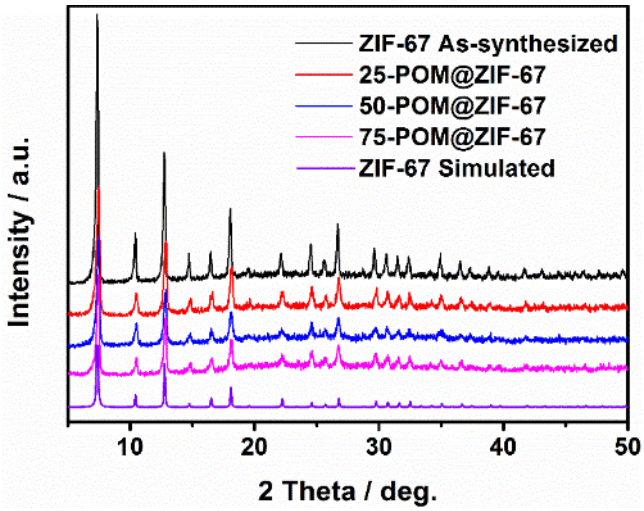

Fig. S1. PXRD patterns of as-synthesized ZIF-67 and POM@ZIF-67 hybrids.

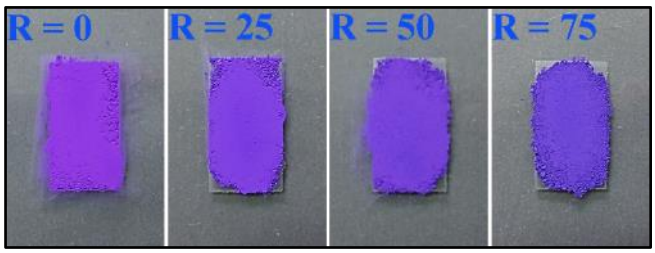

Fig. S2. Color change of POM@ZIF-67 hybrids with the increment of POM feeding amounts.

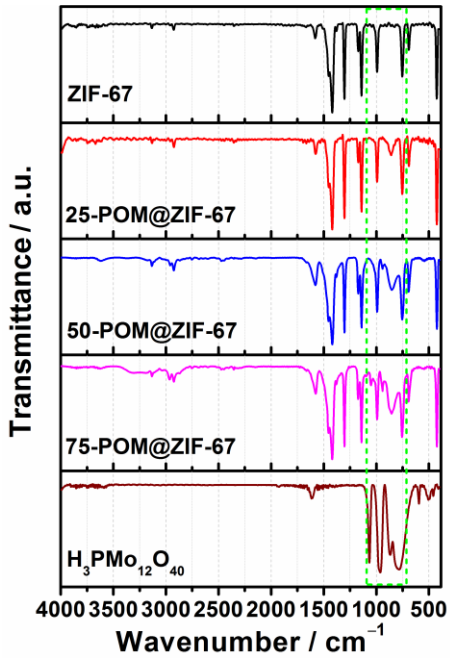

Fig. S3. FTIR spectra of $H_3PMo_{12}O_{40}$, ZIF-67 and POM@ZIF-67 hybrids. As shown in the green dash box, compared to the FTIR spectra of pure ZIF-67 and $H_3PMo_{12}O_{40}$, the intensity of peak at 868 cm^{-1} (Mo−O−Mo) in POM@ZIF-67 hybrid is gradually intensified with increment of POM loadings, and both the peaks at 961 cm^{-1} (Mo=O) and 1066 cm^{-1} (PO4) become evident in 75-POM@ZIF-67.

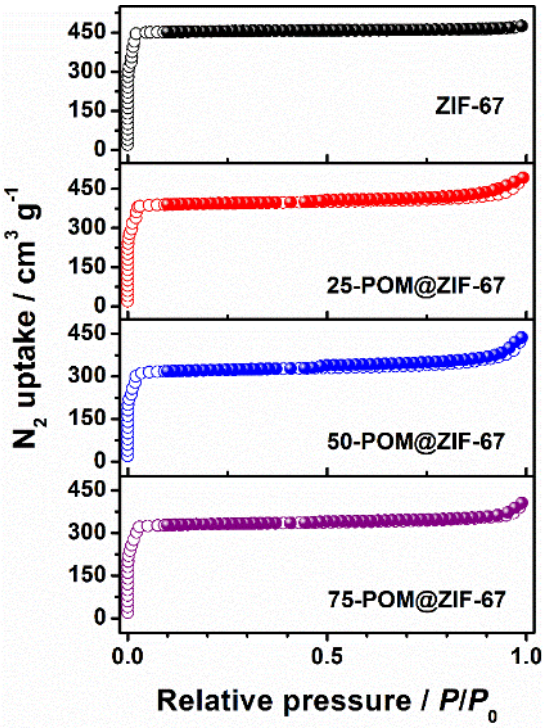

Fig. S4. N_2 sorption isotherms at 77 K for ZIF-67 and POM@ZIF-67 hybrids.

According to elemental analysis and ICP data (**Table S1**), the composition of POM@ZIF-67 with different POM loadings can be expressed as $H_3PMo_{12}O_{40}\subset[Co(C_4H_5N_2)_2]_{140}$, $H_3PMo_{12}O_{40}\subset[Co(C_4H_5N_2)_2]_{66}$ and $H_3PMo_{12}O_{40}\subset[Co(C_4H_5N_2)_2]_{47}$ for R = 25, 50 and 75, respectively. Considering each SOD cage of ZIF-67 consists of 6 cobalt ions, there are *ca*. 23 (140/6), 11 (66/6) and 8 (47/6) SOD cages in 25-POM@ZIF-67, 50-POM@ZIF-67 and 75-POM@ZIF-67, respectively. Thus, POM guests occupy one out of every 23, 11 and 8 SOD cages in 25-POM@ZIF-67, 50-POM@ZIF-67 and 75-POM@ZIF-67, respectively, leaving 22, 10 and 7 SOD cages accessible for N_2 adsorbate. We could assume the volume factors are 0.9565 (22/23), 0.9091 (10/11) and 0.875 (7/8), respectively. Accordingly the mass factors of ZIF-67 (excluding the mass contribution of POMs) in 25-POM@ZIF-67, 50-POM@ZIF-67 and 75-POM@ZIF-67 are 0.9443, 0.8896 and 0.8508, respectively. The multiplication values of their mass factors and volume factors are 0.9032, 0.8087 and 0.7445, respectively, and when multiply these values by the BET surface area of pristine ZIF-67 (1833 $m^2\ g^{-1}$), we can get 1655, 1482 and 1365 $m^2\ g^{-1}$ as the theoretical BET surface areas. They are very close to the experimental BET surface areas of 1642, 1465, and 1323 $m^2\ g^{-1}$, respectively. However, when we simply assume that POMs only contribute to the total mass of each sample without occupying any cages, their calculated surface areas turn to be 1731, 1631 and 1560 $m^2\ g^{-1}$, respectively, which are far from the experimental data. Therefore, it is reasonable to infer that all POMs are encapsulated into the cavities of ZIF-67 in POM@ZIF-67 hybrids.

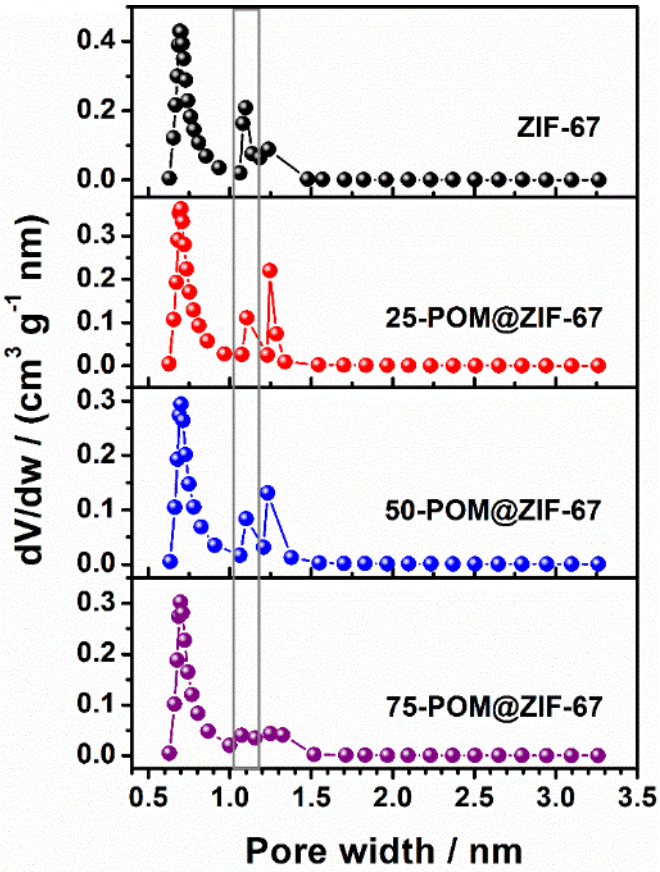

Fig. S5. PSD curves of ZIF-67 and POM@ZIF-67 hybrids calculated by using Horvath-Kawazoe model.

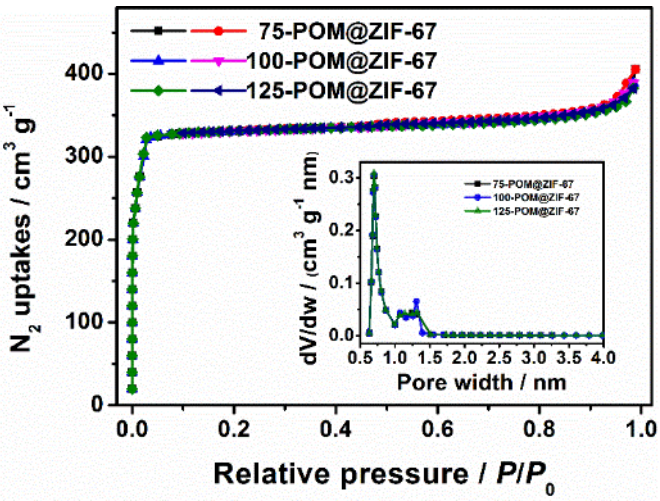

Fig. S6. N_2 sorption isotherms (77 K) and PSD curves of 75-POM@ZIF-67, 100-POM@ZIF-67 and 125-POM@ZIF-67. The PSD are calculated by using Horvath-Kawazoe model.

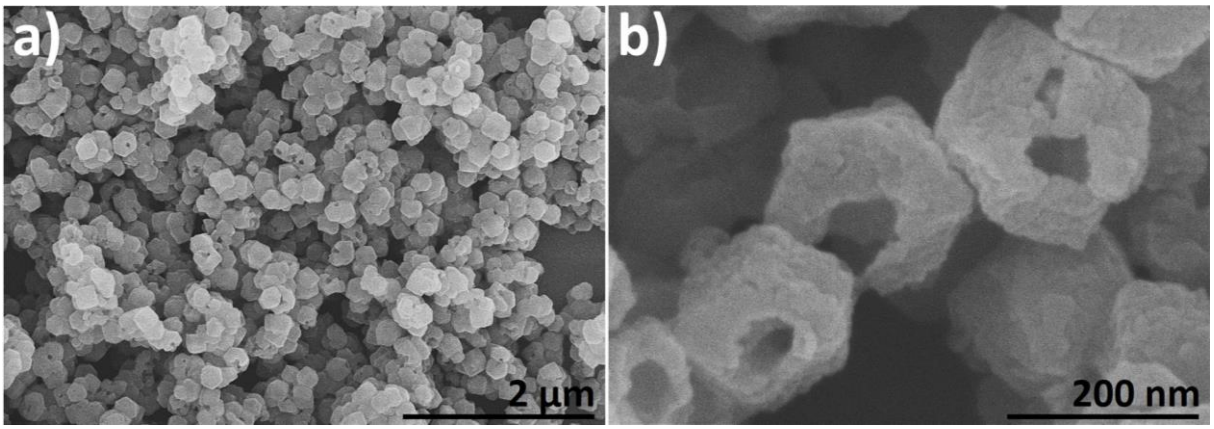

Fig. S7. a) Low and b) high resolution SEM images of 50-POM@ZIF-67.

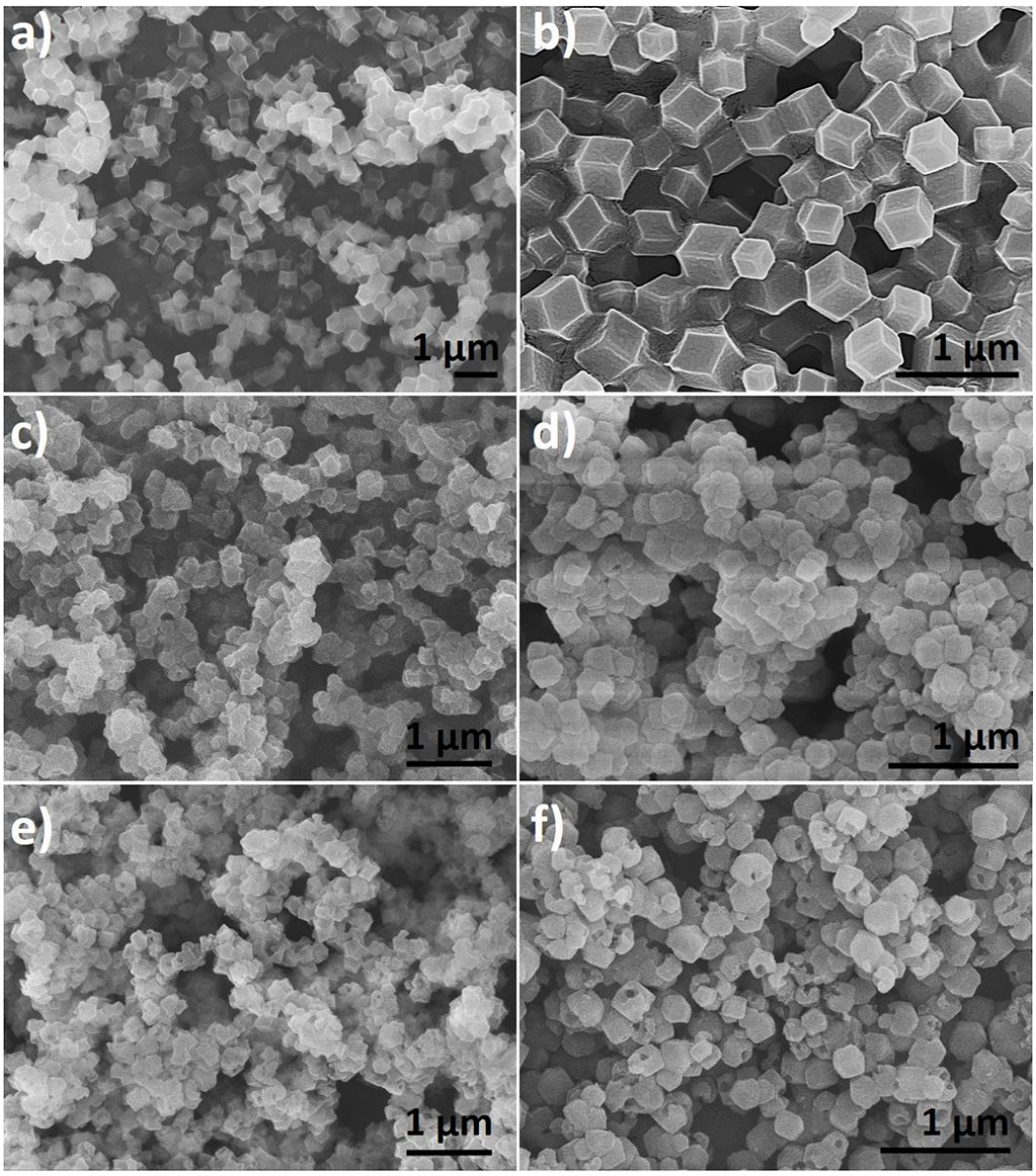

Fig. S8. SEM images of a, b) ZIF-67; c, d) 25-POM@ZIF-67 and e, f) 75-POM@ZIF-67.

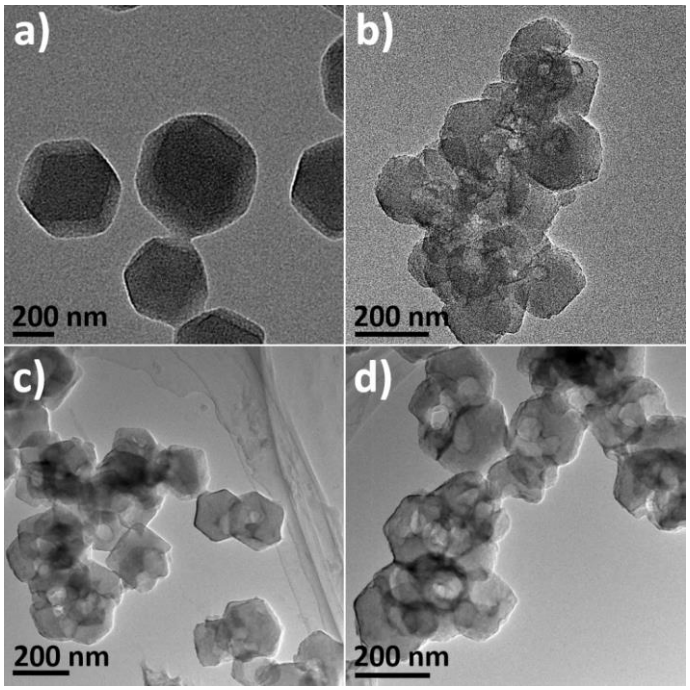

Fig. S9. TEM images of a) ZIF-67; b) 25-POM@ZIF-67; c) 50-POM@ZIF-67; d) 75-POM@ZIF-67.

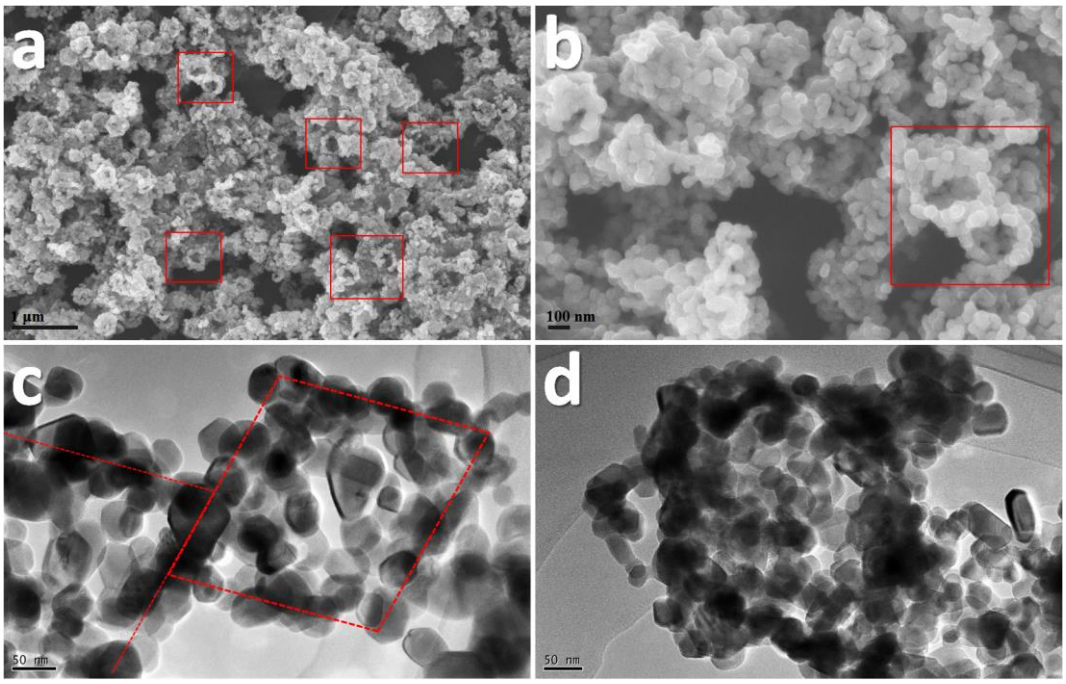

Fig. S10. a, b) SEM and c, d) TEM images of quasi-hollow cage-like structure of Co_3O_4 derived from pristine ZIF-67. The red boxes in panels a and b demonstrate the cage-like structure of Co_3O_4, and the red dash lines in panel c drawn along the densely stacked nanoparticles indicate the frameworks of the cage-like structure.

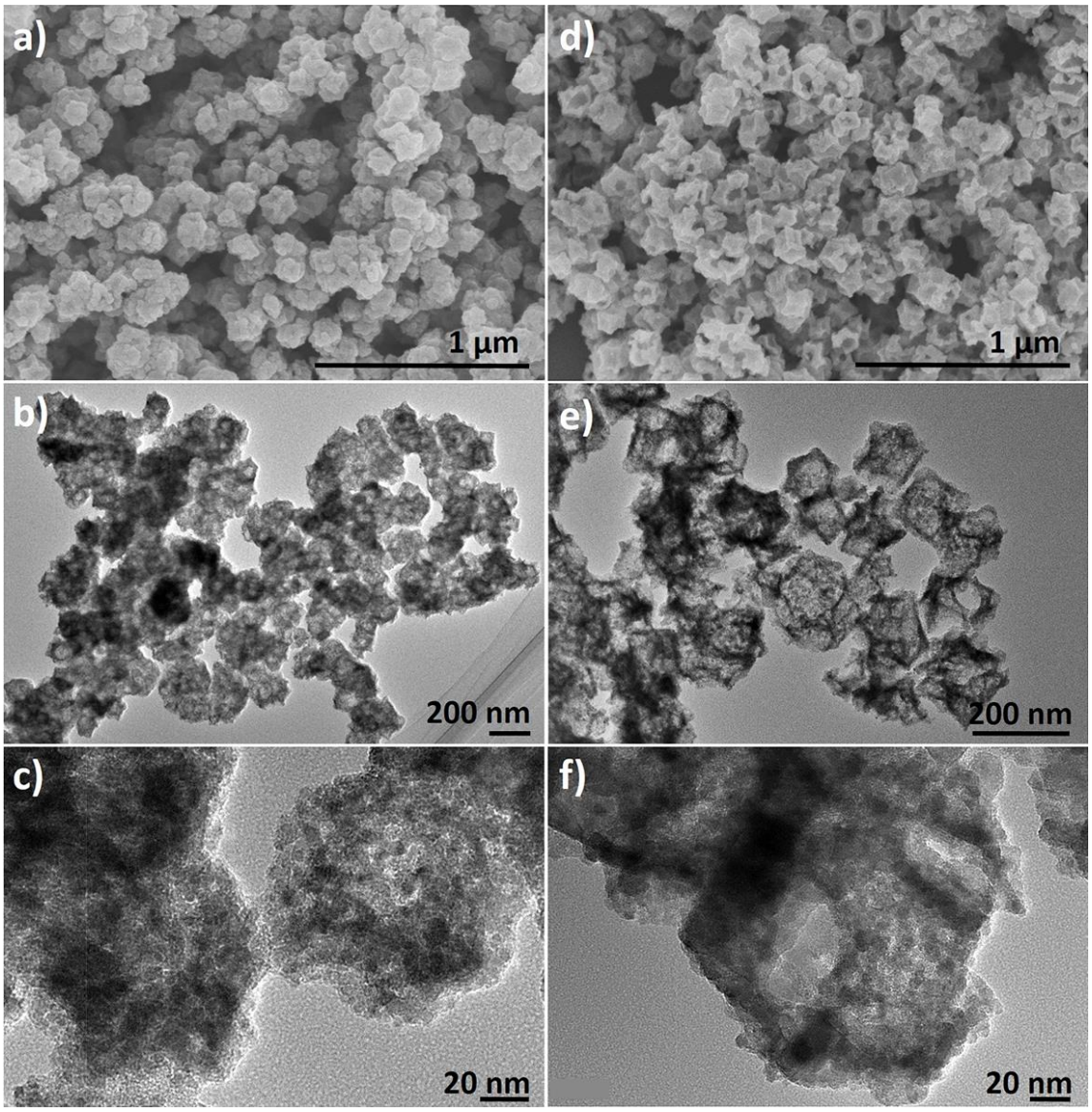

Fig. S11. SEM and TEM images of a–c) $Co_3O_4/CoMoO_4$-25 and d–f) $Co_3O_4/CoMoO_4$-75.

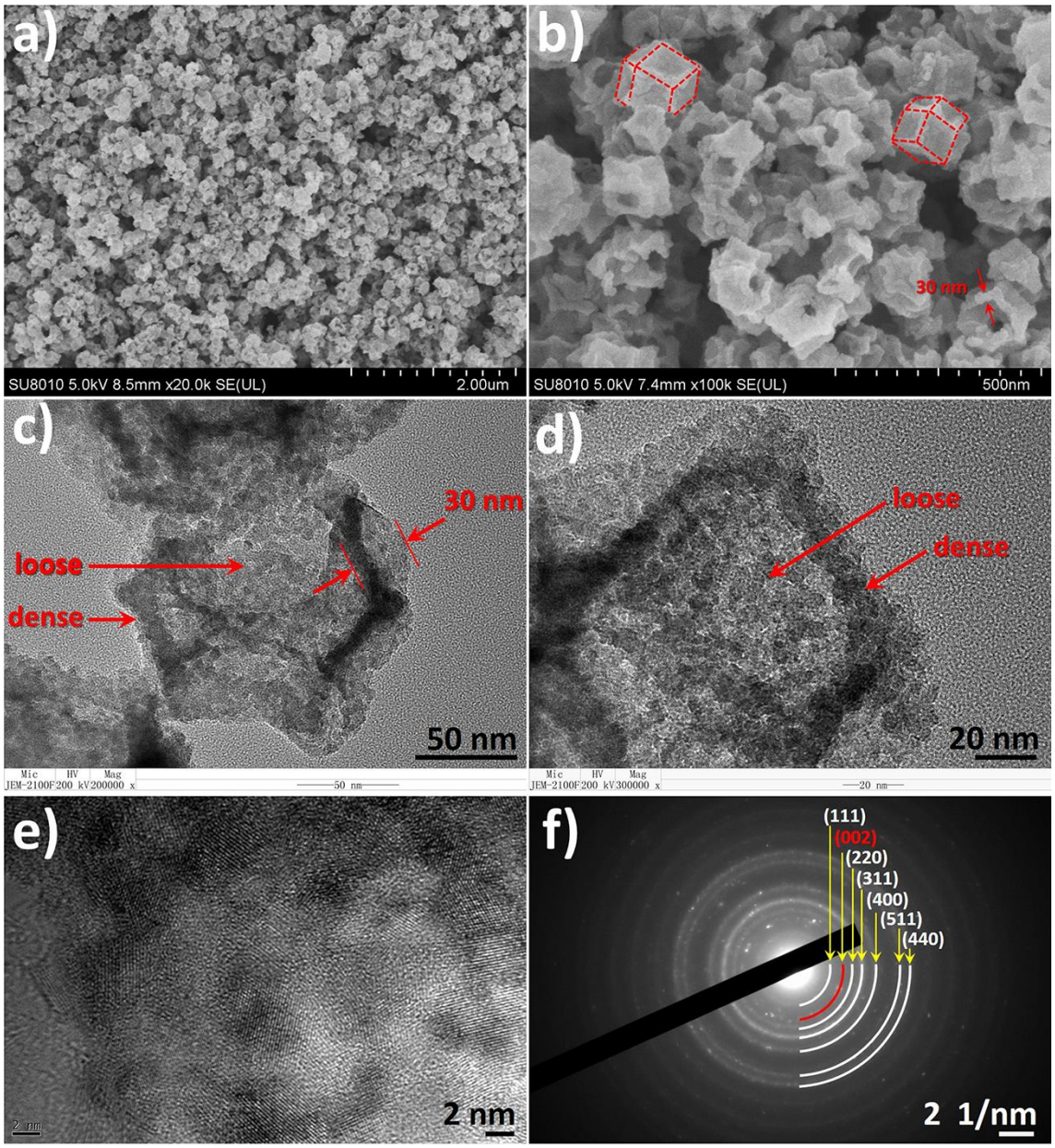

Fig. S12. a) Low and b) high-resolution SEM images of $Co_3O_4/CoMoO_4$-50, the red dash lines and arrows in panel b indicate the better preservation of polyhedron shape of parent POM@ZIF-67 hybrids and shell thickness, respectively; c, d) magnified and e) high-resolution TEM images of $Co_3O_4/CoMoO_4$-50, the red arrows and lines in panel c indicate the shell region is composed of densely stacked nanoparticles and has darker contrast than the void region composed of loosely stacked nanoparticles; f) selective area electron diffraction (SAED) pattern of $Co_3O_4/CoMoO_4$-50, the diffraction rings marked by white and red arcs are indexed to the corresponding lattice planes of Co_3O_4 and $CoMoO_4$, respectively.

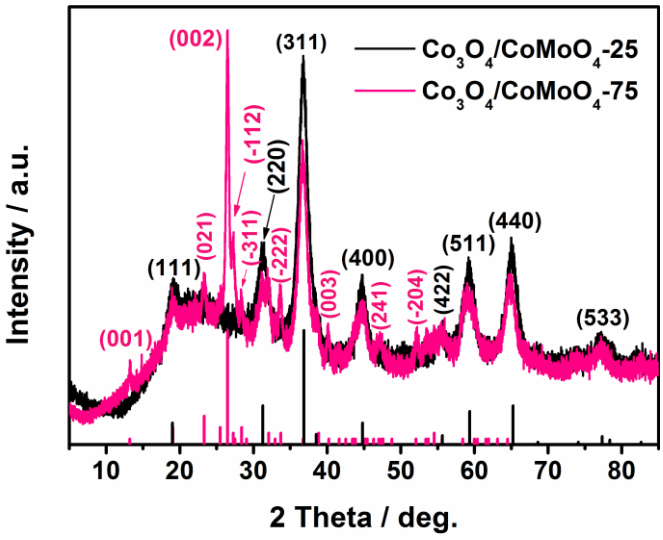

Fig. S13. PXRD patterns of $Co_3O_4/CoMoO_4$-25 and $Co_3O_4/CoMoO_4$-75. The vertical lines in black and pink are the simulated diffraction peak positions of cubic Co_3O_4 (JCPDS # 42-1467) and β-$CoMoO_4$ (JCPDS # 21-0868), respectively.

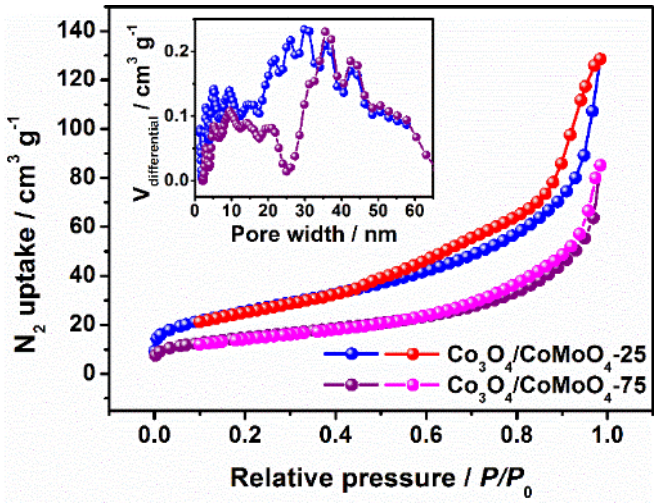

Fig. S14. N_2 sorption isotherms (77 K) and PSD curves of $Co_3O_4/CoMoO_4$-25 and $Co_3O_4/CoMoO_4$-75. The PSD are calculated by using NLDFT model.

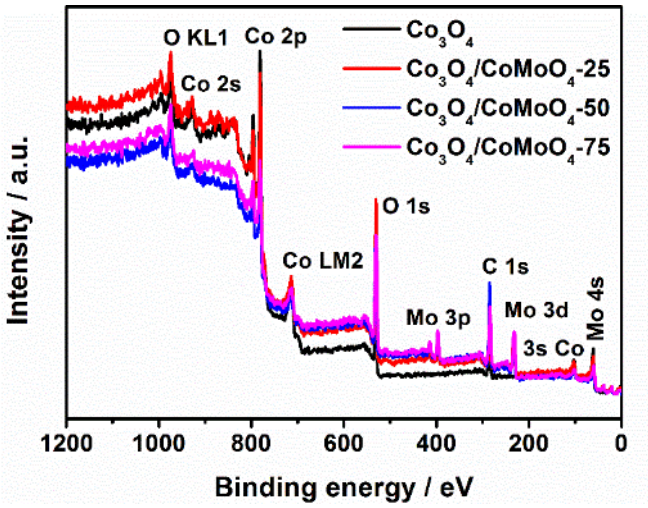

Fig. S15. XPS survey spectra of $Co_3O_4/CoMoO_4$ and Co_3O_4.

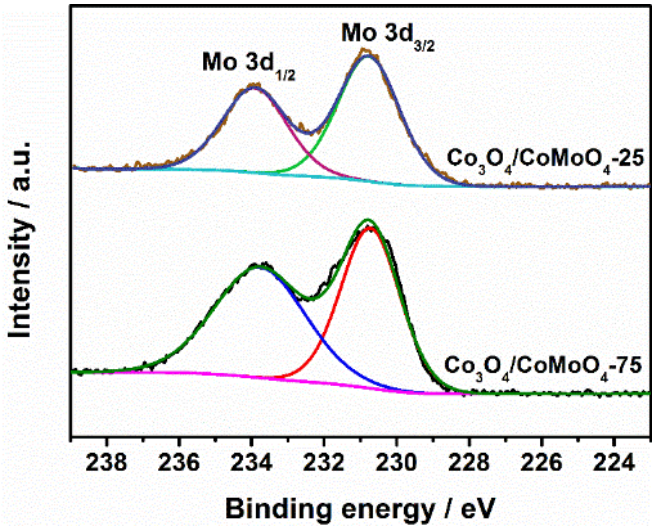

Fig. S16. Mo 3d XPS spectra of $Co_3O_4/CoMoO_4$-25 and $Co_3O_4/CoMoO_4$-75.

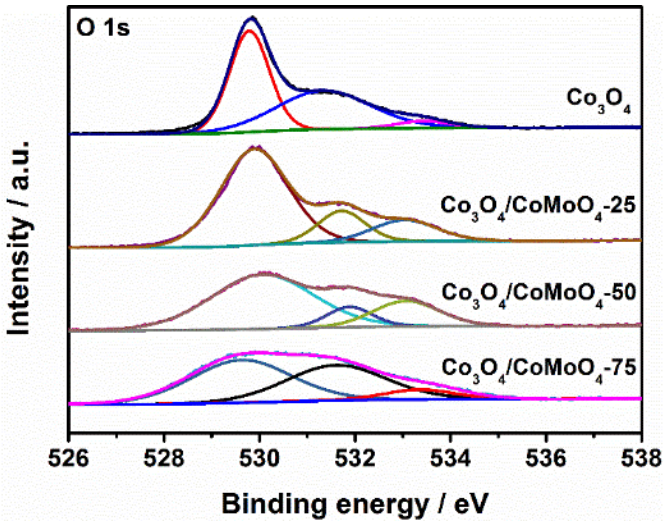

Fig. S17. O 1s XPS spectra of $Co_3O_4/CoMoO_4$ and Co_3O_4.

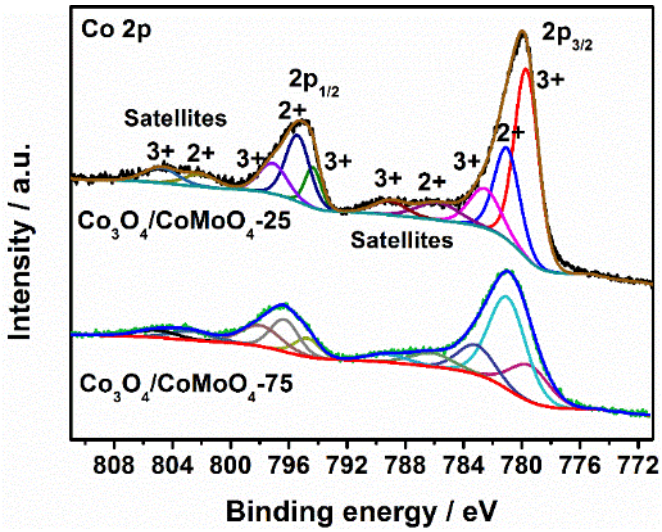

Fig. S18. Co 2p XPS spectra of Co_3O_4/$CoMoO_4$-25 and Co_3O_4/$CoMoO_4$-75.

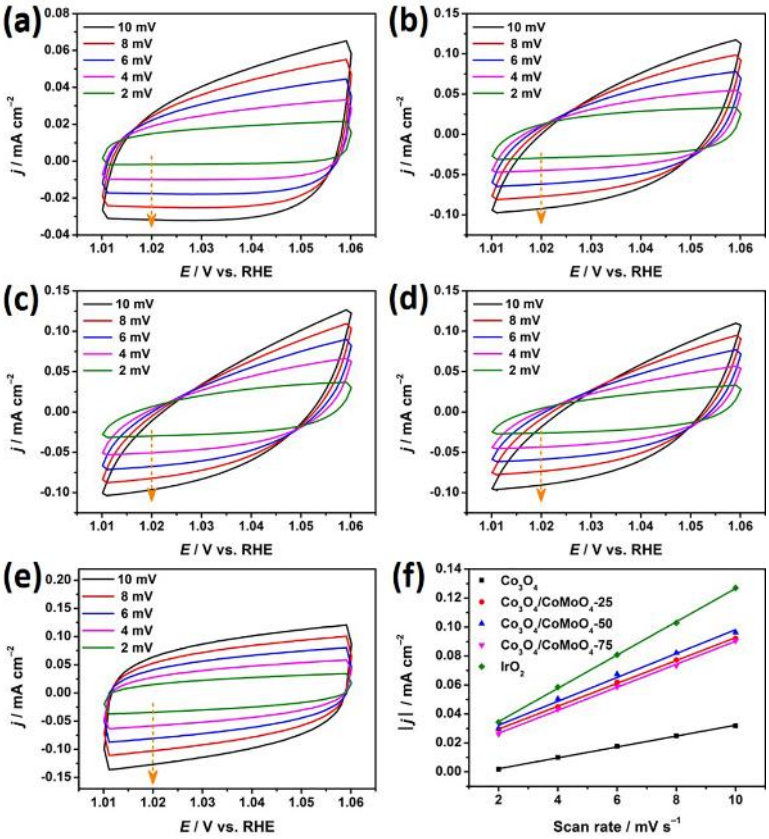

Fig. S19. CVs of a) Co_3O_4, b) Co_3O_4/$CoMoO_4$-25, c) Co_3O_4/$CoMoO_4$-50, d) Co_3O_4/$CoMoO_4$-75 and e) IrO_2 performed in the non-Faradaic region of 1.01 to 1.06 V with various scan rates. (f) The capacitive current density at 1.02 V as a function of scan rate for different catalysts.

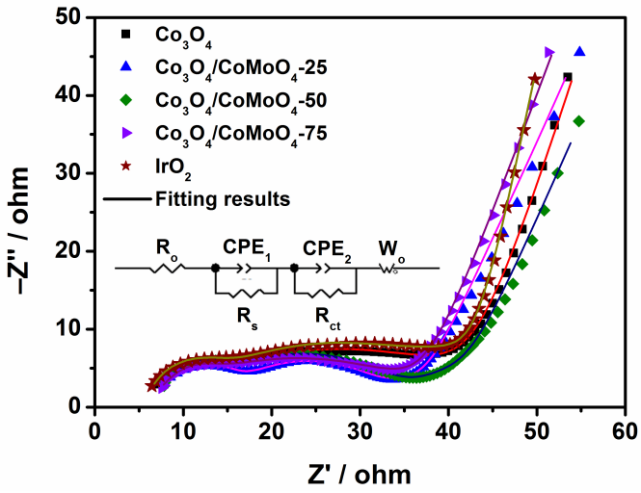

Fig. S20. Nyquist plots of the catalysts obtained by the EIS measurement at a constant potential of 0.2 V. Inset is the simulated equivalent circuit in the form of $R_o(R_s,CPE_1)(R_{ct},CPE_2)W_o$ by fitting the plots using Zview software, the specific data of each circuit element are show in **Table S3**.

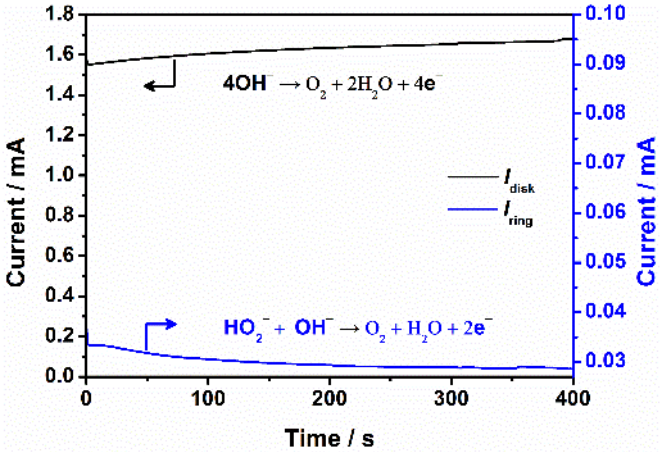

Fig. S21. Evidence of peroxide intermediates generated from $Co_3O_4/CoMoO_4$-50 electrode using RRDE measurement in N_2-purged 1 M KOH solution at 1600 rpm. The HO_2^- generated from $Co_3O_4/CoMoO_4$-50-modified glass carbon disk electrode (current given as I_{disk} @E = 1.53 V) is oxidized at the Pt ring (current given as I_{ring}) at a constant potential of 1.5 V *vs*. RHE.

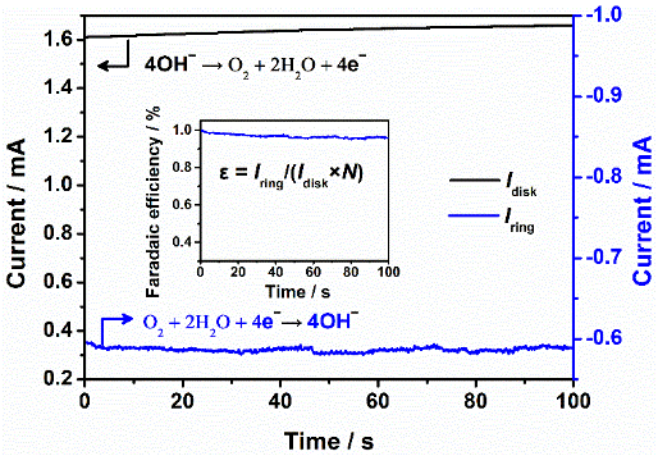

Fig. S22. Evidence of O_2 generated from $Co_3O_4/CoMoO_4$-50 electrode using RRDE measurement in N_2-purged 1 M KOH solution at 1600 rpm. The O_2 generated from $Co_3O_4/CoMoO_4$-50-modified glass carbon disk electrode (OER current given as I_{disk} @E = 1.53 V) is reduced at the Pt ring (ORR current given as I_{ring}) at a constant potential of 0.4 V *vs*. RHE. The inset is the corresponding Faradaic efficiency of $Co_3O_4/CoMoO_4$-50 for OER.

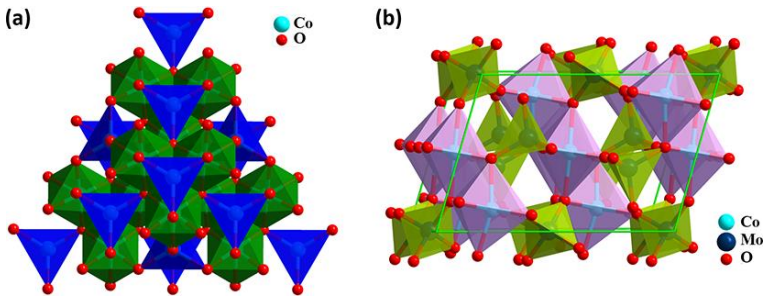

Fig. S23. Microscopic coordination structure in the primary unit cell of a) cubic Co_3O_4 and b) monoclinic β-$CoMoO_4$.

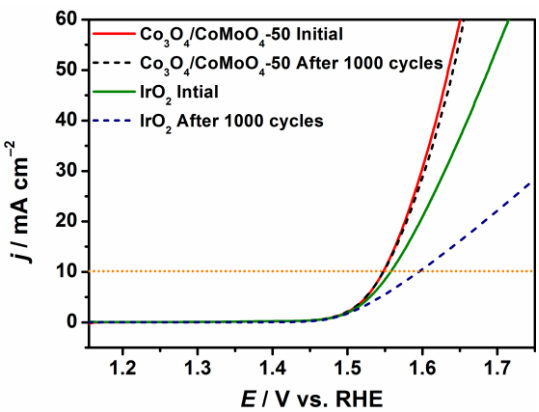

Fig. S24. CVs of $Co_3O_4/CoMoO_4$-50 and IrO_2 measured before and after 1000 cycles.

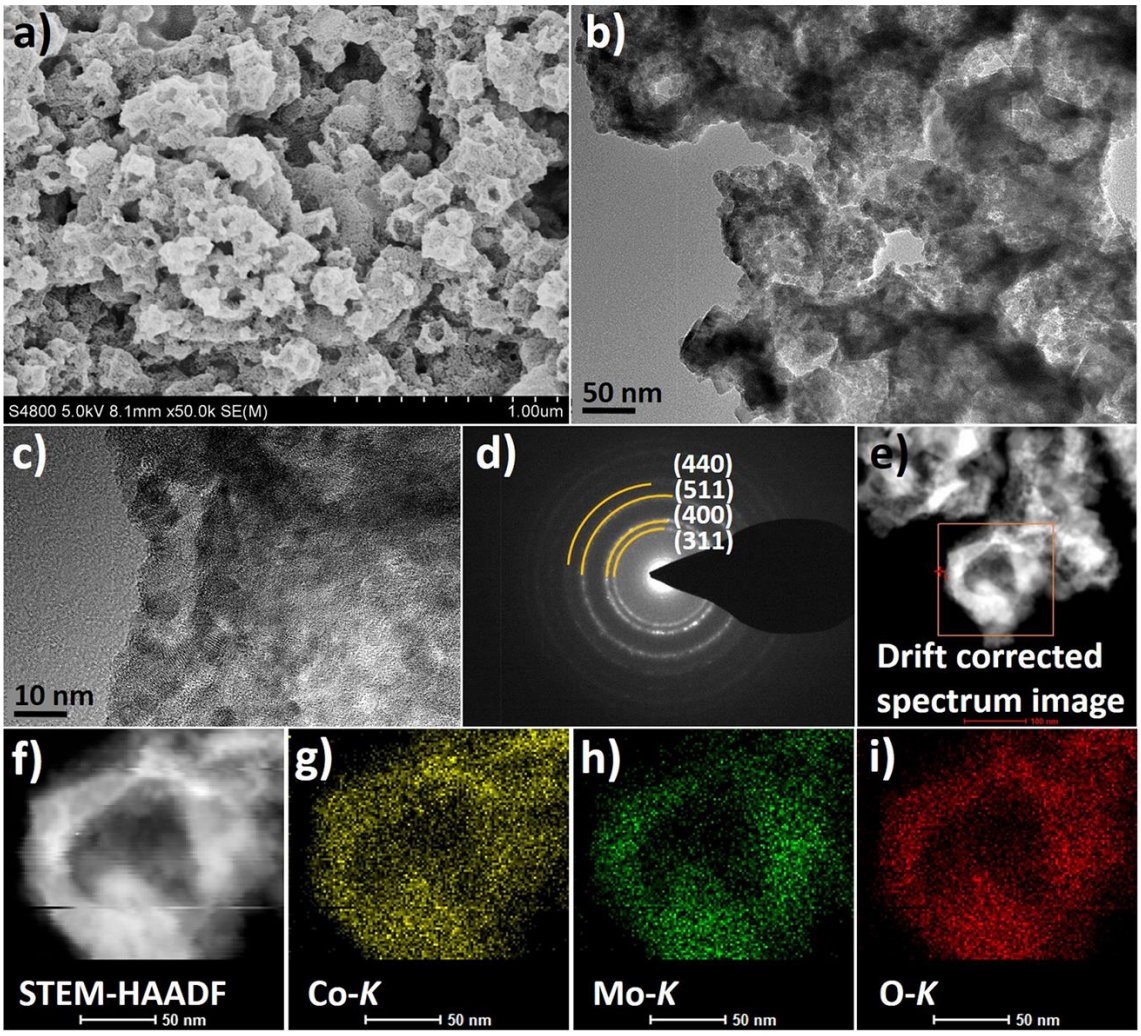

Fig. S25. Electron microscope images of $Co_3O_4/CoMoO_4$-50 after accelerated durability test for 15 h. a) SEM, b) TEM and c) HR-TEM images; d) selected area electron diffraction pattern; e-i) scanning transmission electron microscopy-high angle annular dark field (STEM-HAADF) image and element mappings for Co, Mo and O.

Supplementary Tables

Table S1. Composition and textural properties of ZIF-67, POM@ZIF-67 and the corresponding Co_3O_4 and $Co_3O_4/CoMoO_4$ catalysts.

Samples	C/H/N [wt%]	Co/Mo/P [wt%]	POM loading [wt%]	Mo/Co Ratio	BET SA[a] [m^2 g^{-1}]	V_{total}[b] [cm^3 g^{-1}]
ZIF-67	43.47/4.50/25.21	26.63/0/0	0	0	1833	0.73
25-POM@ZIF-67	39.02/4.19/22.57	24.21/3.39/0.09	5.57	0.140	1642	0.76
50-POM@ ZIF-67	33.59/3.86/19.30	23.51/7.11/0.21	11.04	0.302	1465	0.68
75-POM@ ZIF-67	32.62/3.80/18.85	20.99/8.71/0.23	14.92	0.415	1323	0.63
Co_3O_4	NA	73.42/NA/NA	NA	0	22.5	0.07
$Co_3O_4/CoMoO_4$-25	NA	53.36/7.47/0	NA	0.140	92.6	0.20
$Co_3O_4/CoMoO_4$-50	NA	47.04/14.04/0	NA	0.298	61.3	0.17
$Co_3O_4/CoMoO_4$-75	NA	44.25/18.08/0	NA	0.409	53.7	0.13

[a)]BET surface area calculated by using points between the relative pressures (P/P_0) ranging from 0.01 to 0.1; [b)]Total pore volume measured at relative pressure (P/P_0) of 0.98.

Table S2. Peak binding energies and areas of Co 2p XPS core level.

	Co^{3+} Pair #1		Co^{2+} Pair #1		Co^{3+} Pair #2		Co^{2+} Pair #2		Co^{3+} Pair #3	
	$2p_{3/2}$	$2p_{1/2}$	$2p_{3/2}$	$2p_{1/2}$	$2p_{3/2}$	$2p_{1/2}$	$2p_{3/2}$	$2p_{1/2}$	$2p_{3/2}$	$2p_{1/2}$
Co_3O_4	779.54	794.60	780.89	795.51	782.03	797.17	786.16	802.02	789.58	804.81
	47936.54	17261.30	22373.11	10257.87	21121.25	8245.45	5270.20	1966.36	6403.48	6177.86
$Co_3O_4/CoMoO_4$-25	779.67	794.35	781.02	795.40	782.54	797.09	785.74	802.07	789.08	804.81
	43626.14	6199.20	22110.71	15344.20	11815.91	8208.56	7030.97	3882.42	4374.22	5050.15
$Co_3O_4/CoMoO_4$-50	779.72	794.77	780.64	796.07	782.82	797.64	786.00	802.11	789.21	805.20
	18612.30	7736.04	23550.44	7893.79	6044.61	4586.63	3500.12	3533.16	3183.27	3502.79
$Co_3O_4/CoMoO_4$-75	779.47	794.74	780.99	796.30	783.14	797.94	786.17	802.64	789.25	805.11
	13786.86	4595.62	32825.85	8534.72	10176.01	8206.46	5252.14	3610.84	3282.58	2954.33

All data acquisition and processing were performed using the Thermo Avantage data system, version 5.932. For Co_3O_4 and each $Co_3O_4/CoMoO_4$ composite, the data listed in the first and second lines are corresponding peak binding energy (eV) and area (CPS.eV), respectively. According to the independent total peak areas of Co^{2+} pairs and Co^{3+} pairs, the surface Co^{2+}/Co^{3+} ratio can be calculated as follows:

Co_3O_4:

(22373.11+10257.87+5270.20+1966.36) / (47936.54+17261.30+21121.25+8245.45+6403.48+6177.86)
= 39867.54 / 107145.88 = 0.37

$Co_3O_4/CoMoO_4$-25:

(22110.71+15344.20+7030.97+3882.42) / (43626.14+6199.20+11815.91+8208.56+4374.22+5050.15)
= 48368.3 / 79274.18 = 0.61

$Co_3O_4/CoMoO_4$-50:

(23550.44+7893.79+3500.12+3533.16) / (18612.30+6044.61+7736.04+4586.63+3183.27+3502.79)
= 38477.51/ 43665.64= 0.88

$Co_3O_4/CoMoO_4$-75:

(32825.85+8534.72+5252.14+3610.84) / (13786.86+4595.62+10176.01+8206.46+3282.58+2954.33)
= 50223.55 / 43001.86 = 1.16

Table S3. Comparison of OER activities of different catalysts.

Catalyst	E_{onset}[a] [V]	η_{10}[b] [mV]	Tafel slope [mV dec^{-1}]	J_0[c] [μA cm^{-2}]	C_{dl}[d] [mF cm^{-2}]	TOF [10^{-2} s^{-1}] 320 mV	TOF [10^{-2} s^{-1}] 380 mV
Co_3O_4	1.51	407	83	0.13	3.76	0.36	1.39
$Co_3O_4/CoMoO_4$-25	1.49	341	71	0.20	7.89	1.40	4.42
$Co_3O_4/CoMoO_4$-50	1.47	318	63	0.23	8.23	2.58	7.35
$Co_3O_4/CoMoO_4$-75	1.48	325	64	0.22	7.94	2.08	6.36
IrO_2	1.45	327	53	0.27	11.5	NA	NA

[a]Onset potential, which is defined as the starting point of the linear region of Tafel plot; [b]Overpotential required to obtain the current density of 10 mA cm^{-2}; [c]Exchange current density, which is obtained by extrapolation of the linear region of Tafel plots to the equilibrium potential; [d]Obtained by plotting the cathodic current density at 1.02 V against scan rates by measuring CVs in the non-Faradaic region of 1.01−1.06 V.

Table S4. Fitted parameters of the elements in equivalent circuits for the EIS of different catalysts measured at a constant potential of 0.2 V.

Catalyst	R_o[a] [Ω]	R_s[b] [Ω]	CPE_1[c] [10^{-8}]	n_1[d]	R_{ct}[e] [Ω]	CPE_2 [10^{-5}]	n_2	W_o-R[f] [Ω]	W_o-T	W_o-P
Co_3O_4	4.88	4.31	3.99	0.83	34.87	18.1	0.49	0.68	1.14×10^{-4}	0.42
$Co_3O_4/CoMoO_4$-25	6.98	7.93	5.68	0.97	16.06	3.32	0.71	17.41	0.03	0.38
$Co_3O_4/CoMoO_4$-50	6.85	5.14	1.49	0.98	21.37	2.68	0.66	23.55	0.04	0.38
$Co_3O_4/CoMoO_4$-75	4.92	2.42	1.10	1.00	30.62	16.3	0.48	0.82	1.55×10^{-4}	0.40
IrO_2	5.30	5.69	4.57	1.00	24.97	5.77	0.61	21.26	3.48×10^{-3}	0.45

[a]Combination of intrinsic film resistance of active material and the ionic resistance of the electrolyte; [b]Associated with the contact resistance of the active material/electrode interface layers on the surface of the electrode; [c]Constant phase element; [d]Deviation from the ideal behavior of perfect capacitor (n = 1) or pure resistance (n = 0); [e]Charge transfer resistance; [f]Warburg resistance.

Table S5. Summarization of concentration of the Co ions in different coordination modes for the Co_3O_4 and $Co_3O_4/CoMoO_4$ (The unit of the numbers shown in column 2–6 is μmol g^{-1}).

Catalyst	Co^{3+}	O_h Co^{2+}	T_d Co^{2+}	Co^{3+}+ O_h Co^{2+}+T_d Co^{2+}	Co^{3+} + O_h Co^{2+}	Co^{2+}/Co^{3+}
Co_3O_4	8.3	0	4.15	12.45	8.30	0.50
$Co_3O_4/CoMoO_4$-25	6.6	0.93	3.30	10.83	7.53	0.64
$Co_3O_4/CoMoO_4$-50	5.2	1.73	2.60	9.53	6.93	0.83
$Co_3O_4/CoMoO_4$-75	4.3	2.18	2.17	8.65	6.48	1.01

Table S6. Comparison of OER activities in 1 M KOH solution for the reported MOF-derived catalysts that loaded on a glass carbon electrode.

Catalyst	Loading [μg cm^{-2}]	E_{onset} [V]	η_{10} [mV]	Tafel Slope [mV dec^{-1}]	References
$Co_3O_4/CoMoO_4$-50	255	1.47	318	63	This Work
$Cu_{0.3}Co_{2.7}P$/NC	400	—	190	44	[S1]
CoNi(20 : 1)-P-NS	153	—	273	45	[S2]
Ni@NC-800	310	1.45	280	45	[S3]
A-$CoS_{4.6}O_{0.6}$ PNCs	800	—	290	67	[S4]

$(Ni_{0.62}Fe_{0.38})_2P$	300	1.47	290	44	[S5]
$CoSe_2$	2900	1.48	297	41	[S6]
Ni-P	200	1.48	300	64	[S7]
Co-P/NC	1000	—	319	—	[S8]
Co-P/NC	283	1.50	354	52	[S8]
$Ni_xCo_{3-x}O_{4-y}$ nanocages	357	1.50	320	54	[S9]
$Ni_xCo_{1-x}(OH)_2$ nanosheet	204	1.48	324	33	[S10]
NiCoP/C	255	1.48	330	96	[S11]
Co_9S_8/S-C-800	250	1.51	339	64	[S12]
$Co_3O_4/NiCo_2O_4$ cages	1000	1.53	340	88	[S13]
Co@Co_3O_4@NMCC/rGO	298	1.50	340	71	[S14]
CoP/rGO-400	280	1.50	340	66	[S15]
Fe_3C@NCNT/NPC	918	1.50	340	62	[S16]
CoP@GC	255	1.48	345	56	[S17]
Co-NC/CNT	306	1.51	354	78	[S18]
Co_3ZnC/Co@CN	344	1.50	366	81	[S19]
PNC/Co	350	1.55	370	76	[S20]
Co_3O_4 microframes	286	1.56	370	53	[S21]
NCNTFs	200	1.47	370	93	[S22]
Ni-Co mixed oxide cages	—	1.56	380	50	[S23]
NiS@N/S-C	200	1.54	417	48	[S24]
Co@NCNT	425	1.58	429	116	[S25]
Co_3O_4 polyhedrons	205	1.67	536	57	[S26]

Table S7. Comparison of OER activities in 1 M KOH solution for the recently reported Co-based noble-metal-free catalysts that loaded on a glass carbon electrode.

Catalyst	Loading [μg cm^{-2}]	E_{onset} [V]	η_{10} [mV]	Tafel Slope [mV dec^{-1}]	References
$Co_3O_4/CoMoO_4$-50	**255**	**1.47**	**318**	**63**	**This Work**
$Co_3O_4/CoMoO_4$	240	1.56	370	59	[S27]
$CoMoO_4$	240	1.60	410	84	[S27]
Co_3O_4	136	1.52	400	72	[S28]
G-FeCoW	210	—	217	37	[S29]
CoV_2O_6-V_2O_5/NRGO-1	140	—	239	49.7	[S30]
$Co_{0.7}Fe_{0.3}P$/CNT	500	—	243	36	[S31]
CoFe LDHs-Ar	204	1.457	266	37.85	[S32]
rGO@$CoNiO_x$	200	1.51	280	42	[S33]
CoB_x NS/G	285	1.50	290	53	[S34]
Co_2P/CNT-900	1000	—	292	68	[S35]
γ-CoOOH NS	150	1.47	300	38	[S36]
CoP_2/C	200	1.50	310	50	[S37]
Co/VN	280	1.49	320	55	[S38]
$NiCo_2O_4$ nanosheet	285	1.50	320	30	[S39]
Fe_3O_4@Co_9S_8/rGO	250	1.48	320	55	[S40]
CoP NR/C	710	1.51	320	71	[S41]
Fe-CoOOH/G	200	1.51	330	37	[S42]
CoMnP	284	1.50	330	61	[S43]

Co/CoP-5	220	—	340	79.5	[S44]
$NiCo_{2.7}(OH)_x$	200	1.48	350	65	[S45]
Co-C_3N_4/CNT	408	1.5	380	68.4	[S46]
$CoTe_2$	280	1.52	380	58	[S47]

Supplementary References

[S1] J. Song, C. Zhu, B.Z. Xu, S. Fu, M.H. Engelhard, R. Ye, D. Du, S.P. Beckman, Y. Lin, *Adv. Energy Mater.*, 2017, **7**, 1601555.

[S2] X. Xiao, C.-T. He, S. Zhao, J. Li, W. Lin, Z. Yuan, Q. Zhang, S. Wang, L. Dai, D. Yu, *Energy Environ. Sci.*, 2017, **10**, 893.

[S3] Y. Xu, W. Tu, B. Zhang, S. Yin, Y. Huang, M. Kraft, R. Xu, *Adv. Mater.*, 2017, **29**, 1605957.

[S4] P. Cai, J. Huang, J. Chen, Z. Wen, *Angew. Chem., Int. Ed.*, 2017, **56**, 4858.

[S5] H.-H. Zou, C.-Z. Yuan, H.-Y. Zou, T.-Y. Cheang, S.-J. Zhao, U.Y. Qazi, S.-L. Zhong, L. Wang, A.-W. Xu, *Catal. Sci. Technol.*, 2017, **7**, 1549.

[S6] C. Sun, Q. Dong, J. Yang, Z. Dai, J. Lin, P. Chen, W. Huang, X. Dong, *Nano Res.*, 2016, **9**, 2234.

[S7] X.-Y. Yu, Y. Feng, B. Guan, X.W. Lou, U. Paik, *Energy Environ. Sci.*, 2016, **9**, 1246.

[S8] B. You, N. Jiang, M. Sheng, S. Gul, J. Yano, Y. Sun, *Chem. Mater.*, 2015, **27**, 7636.

[S9] R. P. Antony, A. K. Satpati, K. Bhattacharyya, B. N. Jagatap, *Adv. Mater. Interfaces*, 2016, **3**, 1600632.

[S10] K. He, Z. Cao, R. Liu, Y. Miao, H. Ma, Y. Ding, *Nano Res.*, 2016, **9**, 1856.

[S11] P. He, X.-Y. Yu, X.W. Lou, *Angew. Chem., Int. Ed.*, 2017, **56**, 3897.

[S12] H. Qian, J. Tang, Z. Wang, J. Kim, J. H. Kim, S. M. Alshehri, E. Yanmaz, X. Wang, Y. Yamauchi, *Chem.-Eur. J.,* 2016, **22**, 18259.

[S13] H. Hu, B. Guan, B. Xia, X. W. Lou, *J. Am. Chem. Soc.*, 2015, **137**, 5590.

[S14] X. Li, Y. Fang, L. Wen, F. Li, G. Yin, W. Chen, X. An, J. Jin, J. Ma, *Dalton Trans.,* 2016, **45**, 5575.

[S15] L. Jiao, Y.-X. Zhou, H.-L. Jiang, *Chem. Sci.,* 2016, **7**, 1690.

[S16] P. Zhao, X. Hua, W. Xu, W. Luo, S. Chen, G. Cheng, *Catal. Sci. Technol.*, 2016, **6**, 6365.

[S17] R. Wu, D. Wang, K. Zhou, N. Srikanth, J. Wei, Z. Chen, *J. Mater. Chem. A*, 2016, **4**, 13742.

[S18] F. Yang, P. Zhao, X. Hua, W. Luo, G. Cheng, W. Xing, S. Chen, *J. Mater. Chem. A*, 2016, **4**, 16057.

[S19] J. Su, G. Xia, R. Li, Y. Yang, J. Chen, R. Shi, P. Jiang, Q. Chen, *J. Mater. Chem. A*, 2016, **4**, 9204.

[S20] X. Li, Z. Niu, J. Jiang, L. Ai, *J. Mater. Chem. A*, 2016, **4**, 3204.

[S21] Y. Feng, X.-Y. Yu, U. Paik, *Chem. Commun.,* 2016, **52**, 6269.

[S22] B.Y. Xia, Y. Yan, N. Li, H.B. Wu, X.W. Lou, X. Wang, *Nat. Energy*, 2016, **1**, 15006.

[S23] L. Han, X.-Y. Yu, X. W. Lou, *Adv. Mater.*, 2016, **18**, 4601.

[S24] L. Yang, M. Gao, B. Dai, X. Guo, Z. Liu, B. Peng, *Electrochim. Acta,* 2016, **191**, 813.

[S25] E. Zhang, Y. Xie, S. Ci, J. Jia, P. Cai, L. Yi, Z. Wen, *J. Mater. Chem. A*, 2016, **4**, 17288.

[S26] D. Dong, Y. Liu, J. Li, *Part. Part. Syst. Char.*, 2016, **33**, 887.

[S27] Y. Yang, S. Wang, C. Jiang, Q. Lu, Z. Tang, X. Wang, *Chem. Mater.*, 2016, **28**, 2417.

[S28] Y. Wang, T. Zhou, K. Jiang, P. Da, Z. Peng, J. Tang, B. Kong, W.-B. Cai, Z. Yang, G. Zheng, *Adv. Energy Mater.,* 2014, **4**, 1400696.

[S29] B. Zhang, X. Zheng, O. Voznyy, R. Comin, M. Bajdich, M. García-Melchor, L. Han, J. Xu, M. Liu, L. Zheng, F.P. García de Arquer, C.T. Dinh, F. Fan, M. Yuan, E. Yassitepe, N. Chen, T. Regier, P. Liu, Y. Li, P. De Luna, A. Janmohamed, H.L. Xin, H. Yang, A. Vojvodic, E.H. Sargent, *Science*, 2016, **352**, 333.

[S30] F.-C. Shen, Y. Wang, Y.-J. Tang, S.-L. Li, Y.-R. Wang, L.-Z. Dong, Y.-F. Li, Y. Xu, Y.-Q. Lan, *ACS Energy Lett.*, 2017, **2**, 1327.

[S31] X. Zhang, X. Zhang, H. Xu, Z. Wu, H. Wang, Y. Liang, *Adv. Funct. Mater.*, 2017, **27**, 1606635.

[S32] Y. Wang, Y. Zhang, Z. Liu, C. Xie, S. Feng, D. Liu, M. Shao, S. Wang, *Angew. Chem., Int. Ed.,* 2017, **56**, 5867.

[S33] P. Li, H.C. Zeng, *Adv. Funct. Mater*., 2017, **27**, 1606325.

[S34] P. Chen, K. Xu, T. Zhou, Y. Tong, J. Wu, H. Cheng, X. Lu, H. Ding, C. Wu, Y. Xie, *Angew. Chem. Int. Ed*., 2016, **55**, 2488.

[S35] D. Das, K.K. Nanda, *Nano Energy*, 2016, **30**, 303.

[S36] J. Huang, J. Chen, T. Yao, J. He, S. Jiang, Z. Sun, Q. Liu, W. Cheng, F. Hu, Y. Jiang, Z. Pan, S. Wei, *Angew. Chem., Int. Ed*., 2015, **54**, 8722.

[S37] A. Dutta, A.K. Samantara, S.K. Dutta, B.K. Jena, N. Pradhan, *ACS Energy Lett*., 2016, **1**, 169.

[S38] X. Peng, L. Wang, L. Hu, Y. Li, B. Gao, H. Song, C. Huang, X. Zhang, J. Fu, K. Huo, P.K. Chu, *Nano Energy*, 2017, **34**, 1.

[S39] J. Bao, X. Zhang, B. Fan, J. Zhang, M. Zhou, W. Yang, X. Hu, H. Wang, B. Pan, Y. Xie, *Angew. Chem. Int. Ed*., 2015, **54**, 7399.

[S40] J. Yang, G. Zhu, Y. Liu, J. Xia, Z. Ji, X. Shen, S. Wu, *Adv. Funct. Mater.*, 2016, **26**, 4712.

[S41] J. Chang, Y. Xiao, M. Xiao, J. Ge, C. Liu, W. Xing, *ACS Catal*., 2015, **5**, 6874.

[S42] X. Han, C. Yu, S. Zhou, C. Zhao, H. Huang, J. Yang, Z. Liu, J. Zhao, J. Qiu, *Adv. Energy Mater.*, 2017, **7**, 1602148.

[S43] D. Li, H. Baydoun, C. N. Verani, S. L. Brock, *J. Am. Chem. Soc*., 2016, **138**, 4006.

[S44] Z.-H. Xue, H. Su, Q.-Y. Yu, B. Zhang, H.-H. Wang, X.-H. Li, J.-S. Chen, *Adv. Energy Mater*., 2017, **7**, 1602355.

[S45] J. Nai, H. Yin, T. You, L. Zheng, J. Zhang, P. Wang, Z. Jin, Y. Tian, J. Liu, Z. Tang, L. Guo, *Adv. Energy Mater.,* 2015, **5**, 1401880.

[S46] Y. Zheng, Y. Jiao, Y. Zhu, Q. Cai, A. Vasileff, L.H. Li, Y. Han, Y. Chen, S.-Z. Qiao, *J. Am. Chem. Soc*., 2017, **139**, 3336.

[S47] I. G. McKendry, A. C. Thenuwara, J. Sun, H. Peng, J. P. Perdew, D. R. Strongin, M. J. Zdilla, *ACS Catal*., 2016, **6**, 7393.